Cell Metabolism
Article

MICU1 Controls Both the Threshold and Cooperative Activation of the Mitochondrial Ca^{2+} Uniporter

György Csordás,[1,8] Tünde Golenár,[1,8] Erin L. Seifert,[1,8] Kimberli J. Kamer,[2] Yasemin Sancak,[2,3] Fabiana Perocchi,[2,3,6] Cynthia Moffat,[1] David Weaver,[1] Sergio de la Fuente Perez,[1] Roman Bogorad,[4] Victor Koteliansky,[5,7] Jeffrey Adijanto,[1] Vamsi K. Mootha,[2,3,*] and György Hajnóczky[1,*]

[1]Department of Pathology, Anatomy, and Cell Biology, Thomas Jefferson University, Philadelphia, PA 19107, USA
[2]Department of Molecular Biology, Massachusetts General Hospital, Boston, MA 02114, USA
[3]Department of Systems Biology, Harvard Medical School and Broad Institute, Cambridge, MA 02142, USA
[4]Koch Institute for Integrative Cancer Research, Massachusetts Institute of Technology, Cambridge, MA 02139, USA
[5]Alnylam Pharmaceuticals Inc., Cambridge, MA 02142, USA
[6]Gene Center, Ludwig-Maximilians-Universität, Munich D-81377, Germany
[7]Present address: Koch Institute for Integrative Cancer Research, Massachusetts Institute of Technology, Cambridge, MA 02139, USA
[8]These authors contributed equally to this work
*Correspondence: vamsi@hms.harvard.edu (V.K.M.), gyorgy.hajnoczky@jefferson.edu (G.H.)
http://dx.doi.org/10.1016/j.cmet.2013.04.020

SUMMARY

Mitochondrial Ca^{2+} uptake via the uniporter is central to cell metabolism, signaling, and survival. Recent studies identified MCU as the uniporter's likely pore and MICU1, an EF-hand protein, as its critical regulator. How this complex decodes dynamic cytoplasmic $[Ca^{2+}]$ ($[Ca^{2+}]_c$) signals, to tune out small $[Ca^{2+}]_c$ increases yet permit pulse transmission, remains unknown. We report that loss of MICU1 in mouse liver and cultured cells causes mitochondrial Ca^{2+} accumulation during small $[Ca^{2+}]_c$ elevations but an attenuated response to agonist-induced $[Ca^{2+}]_c$ pulses. The latter reflects loss of positive cooperativity, likely via the EF-hands. MICU1 faces the intermembrane space and responds to $[Ca^{2+}]_c$ changes. Prolonged MICU1 loss leads to an adaptive increase in matrix Ca^{2+} binding, yet cells show impaired oxidative metabolism and sensitization to Ca^{2+} overload. Collectively, the data indicate that MICU1 senses the $[Ca^{2+}]_c$ to establish the uniporter's threshold and gain, thereby allowing mitochondria to properly decode different inputs.

INTRODUCTION

Measurements of mitochondrial matrix $[Ca^{2+}]$ ($[Ca^{2+}]_m$) in intact cells have revealed that mitochondria respond to hormone- and neurotransmitter-induced $[Ca^{2+}]_c$ signals by robust increases in $[Ca^{2+}]_m$, which, in turn, effectively stimulate oxidative metabolism (Hajnóczky et al., 1995; Jouaville et al., 1999; Pralong et al., 1994; Rizzuto et al., 1994; Robb-Gaspers et al., 1998). Prolonged stimulation of mitochondrial Ca^{2+} uptake in combination with other forms of cellular stress induces Ca^{2+} overload and cell death (Pinton et al., 2001; Szalai et al., 1999). Thus, mitochondrial Ca^{2+} import must be tightly controlled to avoid continuous uptake while also ensuring a rapid response to $[Ca^{2+}]_c$ spikes. Indeed, mitochondrial Ca^{2+} uptake effectively decodes different signal patterns: it responds to frequency-modulated $[Ca^{2+}]_c$ oscillations and tunes out moderate $[Ca^{2+}]_c$ increases (Hajnóczky et al., 1995).

One facet of the mitochondria's ability to decode $[Ca^{2+}]_c$ signals is their strategic localization close to ER/SR Ca^{2+} channels, the source of $[Ca^{2+}]_c$ spikes and oscillations, where they are exposed to high $[Ca^{2+}]_c$ microdomains in the vicinity of activated IP_3 receptors (IP3R) and ryanodine receptors (RyRs). Indeed, favorably localized mitochondria seem to respond to spatially confined $[Ca^{2+}]_c$ sparks and puffs (Marchant et al., 2002; Pacher et al., 2002). The close associations and tethering between mitochondria and ER/SR were demonstrated in both intact live cells and in ultrastructural studies (Csordás et al., 2006; de Brito and Scorrano, 2008; Rizzuto et al., 1998; Szabadkai et al., 2006; Tinel et al., 1999). Most recently, exposure of mitochondria to a local 10 μM $[Ca^{2+}]_c$ rise during IP3R-mediated ER Ca^{2+} release was also documented (Csordás et al., 2010; Giacomello et al., 2010). However, the spatial coupling alone cannot explain the highly cooperative nature of mitochondrial Ca^{2+} uptake. Indeed, Ca^{2+}- and time-dependent activation of mitochondrial Ca^{2+} uptake has been observed (Csordás and Hajnóczky, 2003; Kröner, 1986), but the missing molecular identity of the mitochondrial Ca^{2+} uniporter (mtCU) prevented a better understanding of the nonlinear behavior.

A seminal patch-clamp study of mitoplasts provided evidence that the mtCU is a highly Ca^{2+}-selective ion channel (I_{MiCa}) (Kirichok et al., 2004). Early candidates for the mtCU were mitochondria-localized RyR1 (Beutner et al., 2005) and UCP2/3 (Trenker et al., 2007), but these proteins are not expressed in some tissues displaying robust mtCU activity. Recently, LETM1 was identified as a protein that imports Ca^{2+} by Ca^{2+}/H^+ exchange when $[Ca^{2+}]_m$ is low and is therefore unlikely to contribute to Ca^{2+} uptake as a Ca^{2+} channel (Jiang et al., 2009). A recent landmark study identified and proposed MICU1 as a critical regulator of the mtCU (Perocchi et al., 2010), paving the way to the

molecular identification of MCU as the putative pore-forming component (Baughman et al., 2011; De Stefani et al., 2011). MCU is a transmembrane protein of the inner mitochondrial membrane (IMM) with two predicted transmembrane domains connected by a loop that seems to contribute to the selectivity filter (Baughman et al., 2011; De Stefani et al., 2011). MCU likely oligomerizes to form a pore. MICU1 resides within a complex with MCU and contains a pair of Ca^{2+} binding EF-hand motifs (Baughman et al., 2011; Perocchi et al., 2010). The two proteins exhibit striking coevolution and coexpression (Baughman et al., 2011; Bick et al., 2012) indicating a particularly close functional relationship. Since MICU1 is likely a Ca^{2+}-sensing component of the mtCU, we set out to determine its exact role in the decoding function of mitochondrial Ca^{2+} uptake and its physiological relevance.

We show that upon MICU1 depletion, mitochondrial Ca^{2+} uptake is sensitized to low $[Ca^{2+}]_c$ levels, and the cooperativity of uptake with rising $[Ca^{2+}]_c$ is decreased. We show that MICU1 is associated with the IMM, facing the intermembrane space (IMS) to sense outside Ca^{2+}. Expression of an EF-hand mutant restores the $[Ca^{2+}]_c$ threshold, but not cooperativity. These results suggest that MICU1 controls both $[Ca^{2+}]_c$ threshold and cooperativity of the mtCU, with the latter being dependent on Ca^{2+} binding to MICU1. Furthermore, MICU1-deficient mitochondria fail to effectively respond to short-lasting high-$[Ca^{2+}]_c$ microdomains during calcium oscillations while also failing to ignore submicromolar $[Ca^{2+}]_c$ increases. As a result, MICU1-deficient cells show dysregulation of oxidative metabolism and decreased cell tolerance to stress.

RESULTS

Ca^{2+} Handling in MICU1-Deficient Primary Hepatocytes and HeLa Cells

To test the physiological relevance of MICU1 in calcium signaling, we evaluated $[Ca^{2+}]_c$ and $[Ca^{2+}]_m$ homeostasis in MICU1-deficient hepatocytes. In vivo silencing in mouse liver effectively and specifically decreased MICU1 or MCU mRNA and protein in hepatocytes (see Figure S1A online). Stimulation of hepatocytes with Ca^{2+}-mobilizing agonists elicits $[Ca^{2+}]_c$ spikes and oscillations, which are effectively propagated to mitochondria due to local exposure of mitochondria to high $[Ca^{2+}]_c$ microdomains by adjacent IP3Rs (Hajnóczky et al., 1995; Robb-Gaspers et al., 1998). The $[Ca^{2+}]_c$ rise stimulated by phenylephrine (Figures 1A–1C) or vasopressin (Figure S1D) was unaffected by MICU1 or MCU knockdown, whereas the corresponding $[Ca^{2+}]_m$ response was reduced by MICU1 and abolished by MCU silencing (Figure 1B). At resting $[Ca^{2+}]_c$ ($\leq$100 nM), the $[Ca^{2+}]_m$ was unaltered by depletion of MICU1 or MCU, as determined by a genetically targeted Ca^{2+} reporter (Figure 1C). Furthermore, releasing mitochondrial Ca^{2+} by elimination of the membrane potential ($\Delta\Psi_m$) with an uncoupler (FCCP 5 μM) caused a similar $[Ca^{2+}]_c$ rise in control (Ctrl) and MICU1-deficient cells (MICU1-KD) (Figure S1B).

$[Ca^{2+}]_m$ signals stimulate oxidative metabolism that can be assessed by measurements of the O_2 consumption rate (JO_2). Consistent with an unaltered resting $[Ca^{2+}]_m$, resting JO_2 was found similar in both Ctrl and MICU1-KD (Figure 1D). However, upon IP_3-linked stimulation the increase in JO_2 was relatively small in MICU1-KD, reflecting the blunted $[Ca^{2+}]_m$ rise (Figure 1D).

In contrast to IP_3-linked stimulation, wherein mitochondria are exposed to high Ca^{2+} microdomains, during store-operated Ca^{2+} entry (SOCE) most mitochondria respond to the bulk $[Ca^{2+}]_c$ increase (Hajnóczky et al., 1995). The SOCE-mediated $[Ca^{2+}]_m$ increase appeared early, but the maximum amplitude was blunted in MICU1-KD, while it was greatly suppressed and delayed in MCU-KD (Figure 1E). Plotting $[Ca^{2+}]_m$ against $[Ca^{2+}]_c$ underscores that MICU1-KD cells show a significant $[Ca^{2+}]_m$ increase at lower $[Ca^{2+}]_c$ than Ctrl and further reveals the distinct effects of MICU1 and MCU depletion on the $[Ca^{2+}]_c$ sensitivity of mitochondria (Figure 1E, right).

Similar results were obtained in HeLa cells with stable MICU1-KD (see verification of KD in Figure S1C), where the specificity of the changes associated with MICU1 silencing was validated by rescuing cells by re-expression of MICU1 (Figure 1F). Moreover, simultaneous $[Ca^{2+}]_c$ and $[Ca^{2+}]_m$ measurements in single cells further indicated that relatively low $[Ca^{2+}]_c$ was sufficient to evoke a $[Ca^{2+}]_m$ increase in MICU1-KD (Figure 1G). Ctrl cells showed the onset of the $[Ca^{2+}]_m$ signal in the 0.5–1 μM range of $[Ca^{2+}]_c$, but in most MICU1-KD cells a small $[Ca^{2+}]_m$ increase also occurred at $[Ca^{2+}]_c$ <500 nM (Figure 1G). Consistently, when extracellular $[Ca^{2+}]$ was kept low (0.2 mM $CaCl_2$), the SOCE-induced $[Ca^{2+}]_c$ rise (300–400 nM) evoked a $[Ca^{2+}]_m$ increase in MICU1-KD, but not in Ctrl or MCU-KD (Figure 1H and data not shown). An increase in JO_2 was likewise observed only in the MICU1-KD (Figure 1I, left; resting levels, Figure S1E). However, when higher extracellular $[Ca^{2+}]$ was used to support SOCE, the $[Ca^{2+}]_m$ increase and JO_2 response were larger in the Ctrl (Figures 1F and 1I, right). Thus, stimulation of oxidative metabolism closely follows the MICU1-KD-induced changes in the $[Ca^{2+}]_m$ signal.

The results obtained in both hepatocytes and HeLa cells using several different approaches show that (1) when $[Ca^{2+}]_c$ is maintained at <100 nM by high-affinity plasma membrane and ER Ca^{2+} pumps, the $[Ca^{2+}]_m$ and the amount of matrix Ca^{2+} mobilized by $\Delta\Psi_m$ dissipation are not significantly affected by MICU1 depletion; and (2) $[Ca^{2+}]_m$ signals are attenuated in MICU1-KD, as previously reported (Perocchi et al., 2010); but (3) some $[Ca^{2+}]_m$ rise can be evoked by small $[Ca^{2+}]_c$ increases in MICU1-KD.

$[Ca^{2+}]_m$ reflects the combined contributions of mitochondrial Ca^{2+} fluxes (mtCU-mediated uptake and exchanger-mediated efflux) and Ca^{2+} chelation within the matrix. In intact cells, the mitochondrial Ca^{2+} content can be estimated by the $[Ca^{2+}]_c$ increase evoked by a mitochondrial uncoupler. Addition of FCCP after SOCE resulted in a larger $[Ca^{2+}]_c$ increase in MICU1-KD than in Ctrl (Figures 1J and 1L). The surplus Ca^{2+} is likely sequestered by mitochondria, as the ER Ca^{2+} store was depleted by pretreatment with thapsigargin (Tg), and washout of extracellular Ca^{2+} did not prevent the greater $[Ca^{2+}]_c$ response to FCCP in MICU1-KD versus Ctrl (n = 3, data not shown). Uncoupler-sensitive Ca^{2+} storage must occur during SOCE, since FCCP added before SOCE caused no $[Ca^{2+}]_c$ increase in either MICU1-KD or Ctrl (Figure S1B, Figure 1K). Notably, the SOCE-induced $[Ca^{2+}]_c$ increase after FCCP pretreatment was larger in MICU1-KD than in Ctrl (Figure 1K), indicating an augmented SOCE. The rapid decay of the FCCP-induced Ca^{2+} mobilization

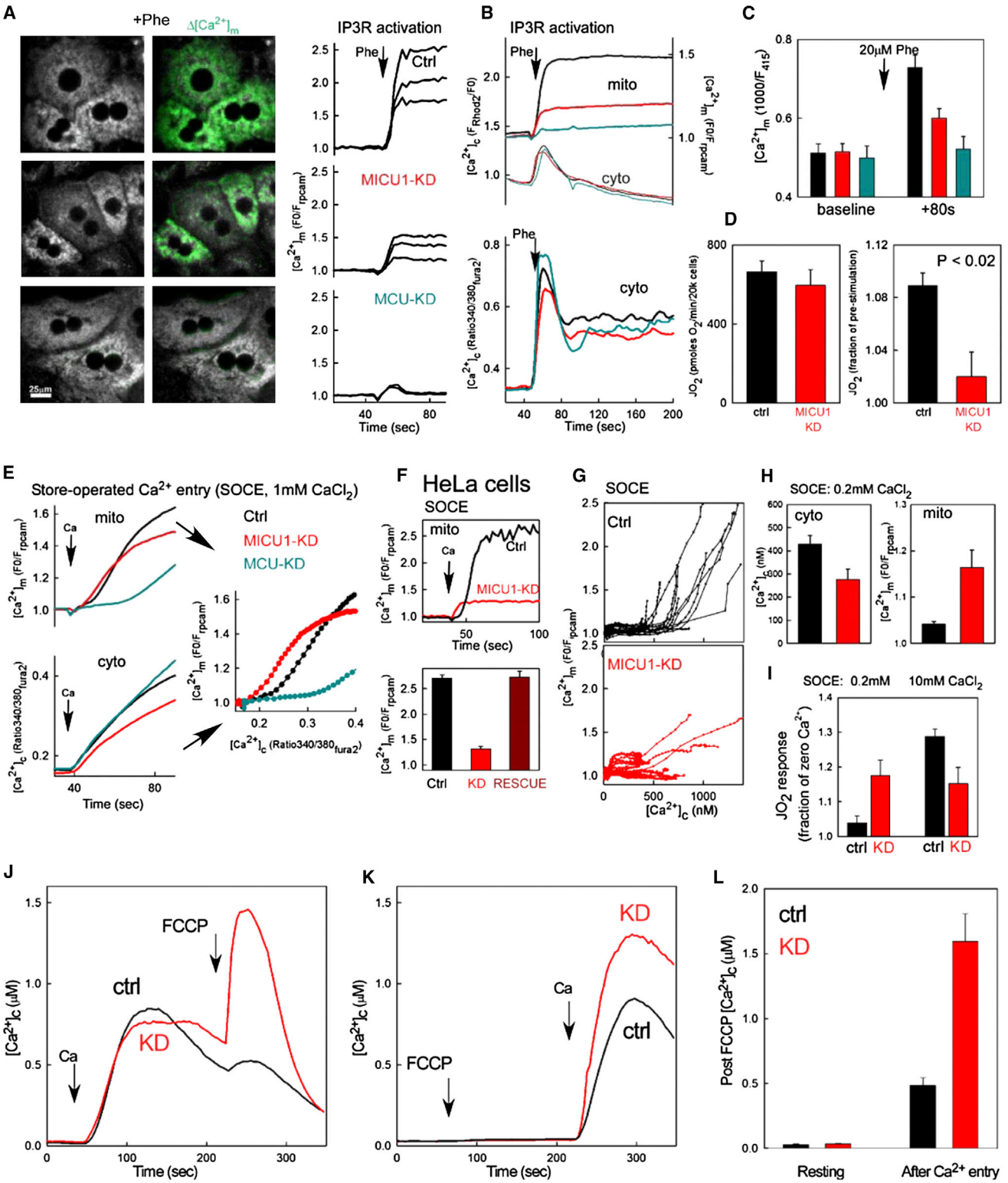

Figure 1. Ca^{2+} Handling in MICU1-KD Hepatocytes and HeLa Cells

(A) Phenylephrine (Phe, 20 μM)-induced $[Ca^{2+}]_m$ signals in control (Ctrl), MICU1-KD, and MCU-KD mouse hepatocytes. (Left) Shown are fluorescence images of mitochondria-targeted ratiometric pericam (mtrpcam) obtained with excitation at the pH-insensitive excitation wavelength (415 nm) overlaid with a green difference image depicting changes during Phe stimulation. (Right) Corresponding $[Ca^{2+}]_m$ time courses. Rpcam fluorescence is inversely normalized to the baseline (F_0/F). (B) Mean $[Ca^{2+}]_c$ and $[Ca^{2+}]_m$ signals obtained by simultaneous recording of rhod2 and mtrpcam fluorescence (n = 43–57 cells, upper) and $[Ca^{2+}]_c$ signals recorded separately using fura2 (n = 71–121, lower).

(legend continued on next page)

(Figure 1J) indicates that the plasma membrane Ca^{2+} pump remains functional and therefore SOCE seems to be upregulated as a consequence of MICU1 depletion. Importantly, inhibition of mitochondrial Ca^{2+} uptake by FCCP pretreatment enhanced the SOCE-induced $[Ca^{2+}]_c$ rise in MICU1-KD, but not in Ctrl (Figure 1K versus Figure 1J), further suggesting that enhanced Ca^{2+} uptake by mitochondria effectively buffers $[Ca^{2+}]_c$ during SOCE in MICU1-KD. Thus MICU1-KD mitochondria avidly take up Ca^{2+} during SOCE, which may be in part due to increased SOCE.

MICU1 Controls the Threshold of Mitochondrial Ca^{2+} Uptake

To directly monitor mitochondrial Ca^{2+} uptake, we measured the ruthenium red (RuRed)-sensitive clearance of Ca^{2+} in the cytoplasmic buffer in suspensions of permeabilized HeLa cells (Figure 2A). When $[Ca^{2+}]_c$ was increased to 30 μM, both Ctrl and MICU1-KD showed rapid clearance (Figure 2A, upper). ER Ca^{2+} uptake could not participate in the Ca^{2+} clearance, since Tg was present. To confirm the appearance of Ca^{2+} in mitochondria, we next quantified the total mitochondrial calcium using ^{45}Ca (Figure S2A). Upon exposure to ~30 μM $[Ca^{2+}]_c$ (100 μM $^{45}CaCl_2$ was added), a massive increase in mitochondrial ^{45}Ca in both Ctrl and MICU1-KD (Figure S2A) confirmed that both MICU1-KD and Ctrl mitochondria effectively take up Ca^{2+} when exposed to supraphysiological Ca^{2+} concentrations.

The results shown in Figure 1 indicated that MICU1-KD mitochondria might actually sequester more Ca^{2+} than normal mitochondria during SOCE that raises $[Ca^{2+}]_c$ to ≤1 μM. To this end, mitochondrial Ca^{2+} uptake was also tested in permeabilized cells exposed to a submicromolar $[Ca^{2+}]_c$ increase (Figure 2A, lower). When $[Ca^{2+}]_c$ was increased to 750 nM, $[Ca^{2+}]_c$ clearance was hardly detectable in Ctrl cells, whereas MICU1-KD mitochondria progressively decreased $[Ca^{2+}]_c$ (Figure 2A, lower). This was abolished by RuRed, confirming the role of mtCU (Figure 2A). Furthermore, simultaneous $[Ca^{2+}]_c$ and $\Delta\Psi_m$ measurements showed that mitochondrial depolarization was apparent at lesser $[Ca^{2+}]_c$ increases in MICU1-KD (Figure S2B). Similar to HeLa cells, in primary hepatocytes, submicromolar $[Ca^{2+}]_c$ elevations elicited progressive Ca^{2+} clearance only in MICU1-KD (Figure 2B).

To determine the lower threshold of mitochondrial Ca^{2+} uptake in MICU1-KD, the steady-state $[Ca^{2+}]_c$ was evaluated in permeabilized cell suspensions (Figure 2C). In Ctrl, the $[Ca^{2+}]_c$ was stabilized at ~400 nM, whereas in MICU1-KD, a lower $[Ca^{2+}]_c$ was attained (Figure 2C, black traces). Addition of RuRed did not affect the steady state in Ctrl, whereas in MICU1-KD a gradual $[Ca^{2+}]_c$ rise took place until the steady-state level of the Ctrl was attained (Figure 2C purple traces). On the other hand, when the exchanger-mediated mitochondrial Ca^{2+} extrusion was inhibited by CGP37157, $[Ca^{2+}]_c$ progressively decreased to <300 nM in MICU1-KD, but not in Ctrl (Figure 2C, green).

These results prompted us to further consider the effect of MICU1-KD on a range of Ca^{2+} doses (Figure 2D). Based on these $[Ca^{2+}]_c$ clearance dose-response curves, mitochondria of Ctrl cells showed steep activation of Ca^{2+} uptake starting at around 1 μM in both HeLa cells and hepatocytes (Figure 2D), consistent with a vast amount of literature. However, in MICU1-KD Ca^{2+} accumulation was detectable well below 1 μM $[Ca^{2+}]_c$. In contrast to MICU1-KD, mitochondria of MCU-KD hepatocytes showed great suppression of Ca^{2+} uptake over the entire $[Ca^{2+}]_c$ range (Figure 2D). These results strongly support the unexpected finding that without MICU1, mitochondrial Ca^{2+} uptake is greatly sensitized to Ca^{2+}.

MICU1 Contributes to Cooperative Activation of the Uniporter

The difference in sigmoidal shape of the $[Ca^{2+}]_c$ dose response for mitochondrial Ca^{2+} uptake in MICU1-KD versus Ctrl in both hepatocytes and HeLa cells (Figure 2D) prompted us to further explore the role of MICU1 in mtCU's cooperativity. To this end, double logarithmic plots of initial Ca^{2+} uptake rates against $[Ca^{2+}]_c$ were created (Figure 3A). MICU1-KD in both hepatocytes and HeLa cells showed significantly lesser slope than their respective controls (Figure 3A; hepatocytes, KD 1.6 ± 0.1, versus Ctrl 2.9 ± 0.3, $p < 0.05$; and HeLa cells, KD 2.1 ± 0.05 versus Ctrl 3.4 ± 0.19, $p < 0.025$). Previous literature has proposed that the cooperativity of mtCU's activation is affected by the presence of Mg^{2+} (Favaron and Bernardi, 1985; Kröner, 1986). Without Mg^{2+}, the difference in slope between Ctrl and MICU1-KD was no longer detectable, and both became similar to MICU1-KD in the presence of Mg^{2+} (Figure 3A, right; KD 2.2 ± 0.1 versus Ctrl 2.3 ± 0.1). This may explain why the effect of MICU1 depletion on the mtCU's cooperativity remained undetected in a recent study performed in Mg^{2+}-free buffer (Mallilankaraman et al., 2012b).

MICU1 is an EF-hand protein and has been proposed as a Ca^{2+} sensor for mitochondrial Ca^{2+} uptake (Perocchi et al., 2010). To test if the Ca^{2+} sensitivity of mtCU is affected by MICU1's EF-hands, we compared mitochondrial Ca^{2+} uptake in Ctrl and MICU1-KD rescued by either wild-type MICU1 (RESCUE) or a MICU1 with both EF-hands mutated to prevent Ca^{2+} binding (ΔEF-RESCUE) (Perocchi et al., 2010). Expression of the rescue constructs was validated by immunoblotting (Figure S3A). Both RESCUE and ΔEF-RESCUE mitochondria

(C) Fluorescence of mtrpcam in resting and Phe-stimulated Ctrl, MICU1-KD, and MCU-KD primary hepatocytes (n = 50–62 from three different mice). Fluorescence values are shown in arbitrary units, inverted but without normalization to allow comparison of the resting $[Ca^{2+}]_m$.
(D) Resting and agonist-stimulated JO_2 in Ctrl and MICU1-KD hepatocytes (n = 4).
(E) SOCE-associated $[Ca^{2+}]_c$ (fura2) and $[Ca^{2+}]_m$ (mtrpcam) signals monitored separately in Ctrl, MICU1-KD, and MCU-KD hepatocytes pretreated with Tg in a Ca^{2+}-free ECM. To evoke SOCE, 1 mM $CaCl_2$ (Ca) was added. (Left) Mean time courses. (Right) $[Ca^{2+}]_m$ versus $[Ca^{2+}]_c$ (n = 144–172 cells for each).
(F) $[Ca^{2+}]_m$ responses to SOCE in Ctrl, MICU1-KD, and RESCUED stable HeLa cells. The mean traces (upper) and mean peak values (lower) of the single cell recordings are shown (n = 16–52 for each).
(G) $[Ca^{2+}]_m$ versus $[Ca^{2+}]_c$ curves of individual Ctrl (top) and MICU1-KD cells (bottom) from similar experiments as in (F).
(H) Mean peak $[Ca^{2+}]_c$ (fura2) and $[Ca^{2+}]_m$ (mtipcam) levels recorded during SOCE induced by addition of 0.2 mM $CaCl_2$ in stable MICU1-KD and Ctrl HeLa cells (n = 16–21).
(I) Measurement of the JO_2 response during SOCE (n = 4 plates/genotype, 3–4 wells/condition/plate).
(J–L) $[Ca^{2+}]_c$ rise caused by FCCP after (J) and before SOCE (K).

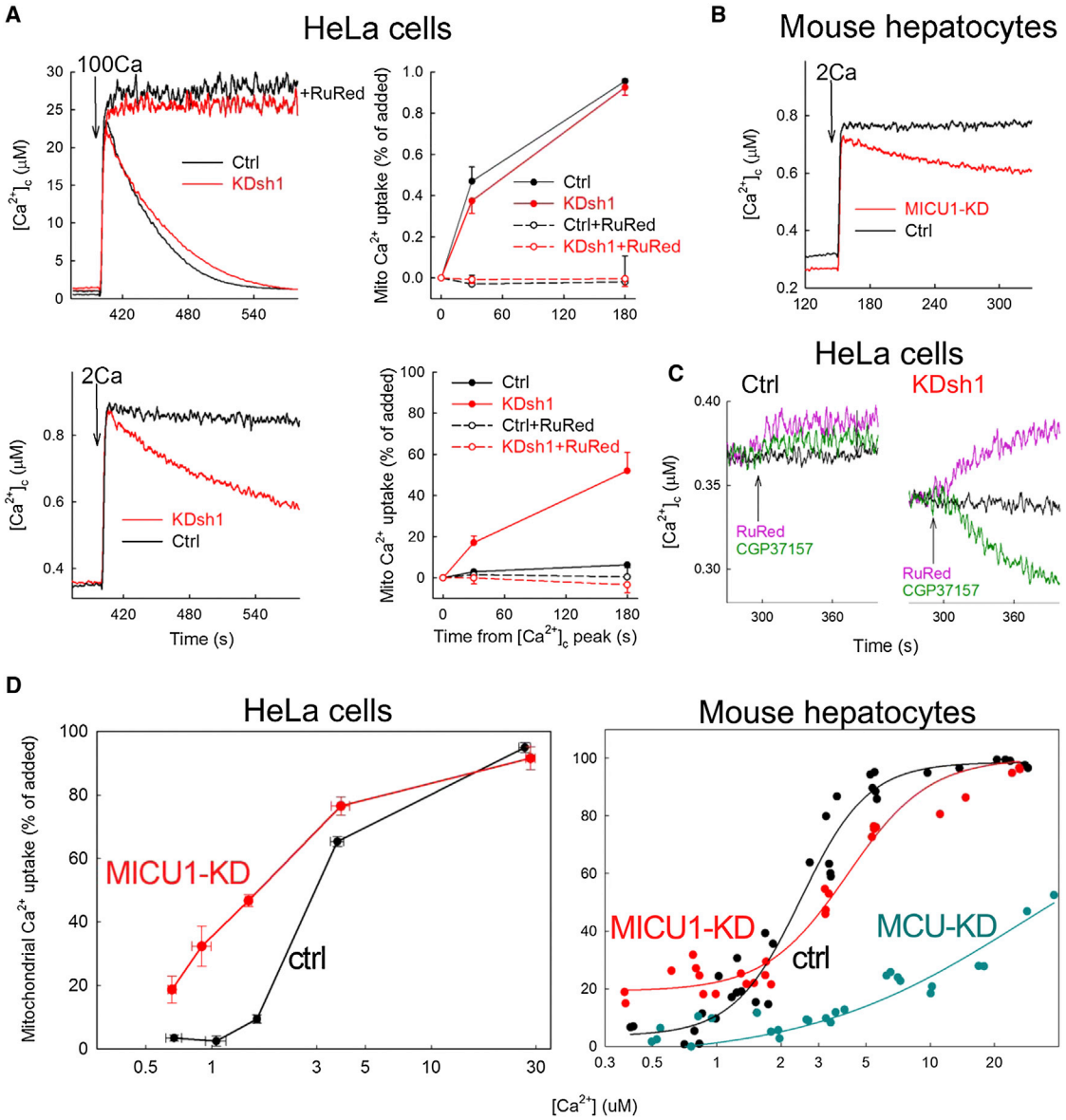

Figure 2. MICU1 Controls the Threshold of Mitochondrial Ca^{2+} Uptake

(A) Clearance of Ca^{2+} added to the cytoplasmic buffer in suspensions of permeabilized HeLa cells incubated in the presence of Tg (2 μM). (Left) Time courses of $[Ca^{2+}]_c$ upon addition of 100 μM (100Ca, upper) or 2 μM (2Ca, lower) $CaCl_2$ to Ctrl (black) and MICU1-KD (red) cells in the absence and presence of RuRed (3 μM). (Right) Mitochondrial Ca^{2+} uptake as the percent recovery of the initial $[Ca^{2+}]_c$ rise 30 s and 180 s after Ca^{2+} addition (means + SEM, n = 11).

(B) Mitochondrial clearance of $[Ca^{2+}]_c$ elevations evoked by 2 μM added $CaCl_2$ in permeabilized Ctrl and MICU1-KD hepatocytes.

(C) Mitochondrial maintenance of basal steady-state $[Ca^{2+}]_c$ in suspensions of permeabilized Ctrl (left) and MICU1-KD (right) HeLa cells as determined by inhibitors of mitochondrial Ca^{2+} uptake (RuRed, pink) and Na^+-dependent extrusion (CGP37157 20 μM, green).

(D) $[Ca^{2+}]_c$ dose response of the mitochondrial Ca^{2+} uptake in HeLa cells (left) and hepatocytes (right), determined as in Figure 2A. The $CaCl_2$ doses added were (in μM) 1, 2, 5, 10, and 100 (n = 4–9). For the hepatocytes, a sigmoid curve fitted to each data set is shown.

were able to take up Ca^{2+} in permeabilized cell assays (Figure S3B); however, while the $[Ca^{2+}]_c$ dose-response curve was similar in RESCUE and Ctrl, a rightward shift and less-steep sigmoidal shape was apparent in ΔEF-RESCUE (Figure 3B). In double logarithmic plots, expression of the wild-type MICU1 construct in MICU1-KD restored the slope observed in the control cells (3.1 ± 0.28), but ΔEF-RESCUE failed to do so (2.5 ± 0.18). Notably, both RESCUE and ΔEF-RESCUE are able to restore the blockade of uptake at low $[Ca^{2+}]_c$. Thus MICU1 is involved in both the closed state and cooperative activation of mtCU, but calcium binding to the EF-hands is not required for promoting closure at low $[Ca^{2+}]_c$ levels and is likely to be relevant in setting the apparent Ca^{2+} affinity of the mtCU via their Ca^{2+} binding. However, a limitation of these experiments is that the Ca^{2+} uptake might be affected by the simultaneous changes in $\Delta\Psi_m$ (see Figure S2B).

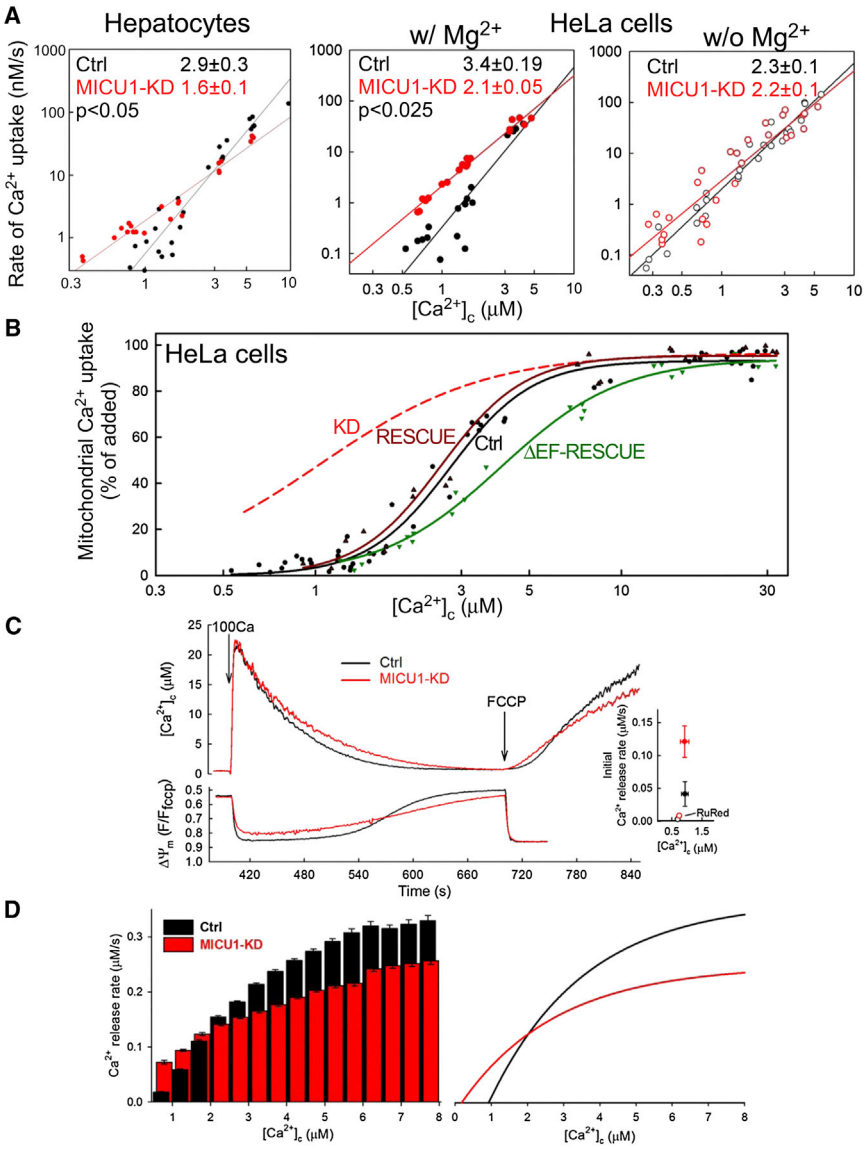

Figure 3. MICU1 Contributes to Cooperative Activation of mtCU

(A) Double logarithmic plots of initial Ca^{2+} uptake rates versus $[Ca^{2+}]_c$ in Ctrl and MICU1-KD hepatocytes and stable HeLa cells in the presence (left and middle) and absence of Mg^{2+} (right). Slope of linear fit for each data set is shown (n = 3).

(B) $[Ca^{2+}]_c$ dose responses of the fractional mitochondrial Ca^{2+} uptake in Ctrl, RESCUE, and ΔEF-RESCUE HeLa cells. Data points from individual recordings (≥3 for each Ca^{2+} dose) and a sigmoid (logistic) fit to each data set are shown. The sigmoid fit for MICU1-KD cells from Figure 2D is shown as a reference (red).

(C) $[Ca^{2+}]_c$ (top) and $\Delta\Psi_m$ (bottom) time courses showing the mitochondrial clearance of a 100 μM $CaCl_2$ pulse (100Ca) and subsequent FCCP-induced Ca^{2+} release in suspensions of permeabilized HeLa cells. (Inset) Mean initial Ca^{2+} release ($[Ca^{2+}]_c$ rise) rates from recordings where, by the time of FCCP addition, $[Ca^{2+}]_c$ dropped below 1.2 μM (means ± SEM, n = 3). Rates obtained from recordings in the presence of RuRed (3 μM) added 30 s before FCCP are shown with open symbol.

(D) (Left) Instantaneous rate of FCCP-induced Ca^{2+} efflux at each $[Ca^{2+}]_c$ (0.5 μM binning) obtained via differentiation of the initial period of the $[Ca^{2+}]_c$ rises (n = 7). (Right) Instantaneous Ca^{2+} release rates extrapolated from compilation of differentiated sigmoidal (logistic) fits. Predicted 0 crossings (the effective thresholds) are 937 and 185 nM for Ctrl and MICU1-KD, respectively.

To avoid such complications, we decided to also assess the $[Ca^{2+}]$ dependence of mtCU-mediated Ca^{2+} efflux in mitochondria of permeabilized cells preloaded with high Ca^{2+} in the presence of Tg. Once $[Ca^{2+}]_c$ returned to near starting levels by mitochondrial uptake, FCCP was added, causing essentially instant dissipation of $\Delta\Psi_m$, followed by an increase in $[Ca^{2+}]_c$ as Ca^{2+} was released from mitochondria (Figure 3C). The initial $[Ca^{2+}]_c$ rise was greatly suppressed by RuRed, confirming that it was mainly a result of mtCU-mediated Ca^{2+} efflux (Figure 3C, inset). When FCCP was added to MICU1-KD cells that had returned $[Ca^{2+}]_c$ to ≤1 μM, the $[Ca^{2+}]_c$ rise started without delay and much faster than in Ctrl cells at similar $[Ca^{2+}]_c$ (Figure 3C). Hence, mitochondrial Ca^{2+} uptake and the ensuing increase in $[Ca^{2+}]_m$ did not abolish the difference in mtCU activation between MICU1-KD and Ctrl. Additionally, MICU1-KD showed nonsigmoidal or less sigmoidal Ca^{2+} release kinetic and smaller maximum rate of $[Ca^{2+}]_c$ rise than the Ctrl (Figure 3C). The double logarithmic plot of initial release rates versus $[Ca^{2+}]_c$ also indicated lesser cooperativity for MICU1-KD than for control (Figure S3C), further supporting the role of MICU1 in activating mtCU. When the FCCP-induced $[Ca^{2+}]_c$ increase traces were combined and the average instantaneous release rates were calculated for a range of $[Ca^{2+}]_c$, the MICU1-KD showed higher rates at <2 μM, but a steeper increase appeared in the Ctrl, with the $[Ca^{2+}]_c$ increase leading to higher maximum rates (Figure 3D, left). MICU1 RESCUE cells likewise showed a steeper increase than ΔEF-RESCUE cells in the Ca^{2+} release rate between 2 and 8 μM $[Ca^{2+}]_c$ as well as a higher maximum rate (Figure S3D), providing evidence that the EF-hands of MICU1 are central to the cooperative activation of the mtCU. Fitting exponential regressions to the complete data sets generated from the experiments (Figure 3D, right) highlights the dual role of MICU1 in keeping mtCU's gate closed at submicromolar $[Ca^{2+}]_c$ and maximizing the Ca^{2+} flux at several μM $[Ca^{2+}]_c$ (Figure 3D, right). The switch between these two effects is likely to be mediated by Ca^{2+} binding to the EF-hands of MICU1. In technical terms, MICU1 operates as a high-pass filter that provides thresholding and gain functions to improve the signal-to-noise ratio. Modeling the fits of Figure 3D as high-pass, "Butterworth" filters, we are able to estimate that in the steep part of the response curve a 10-fold increase in $[Ca^{2+}]_c$ would result in an ~85-fold increase in the rate of Ca^{2+} release in Ctrl, compared with only an ~4× increase in MICU1-KD cells.

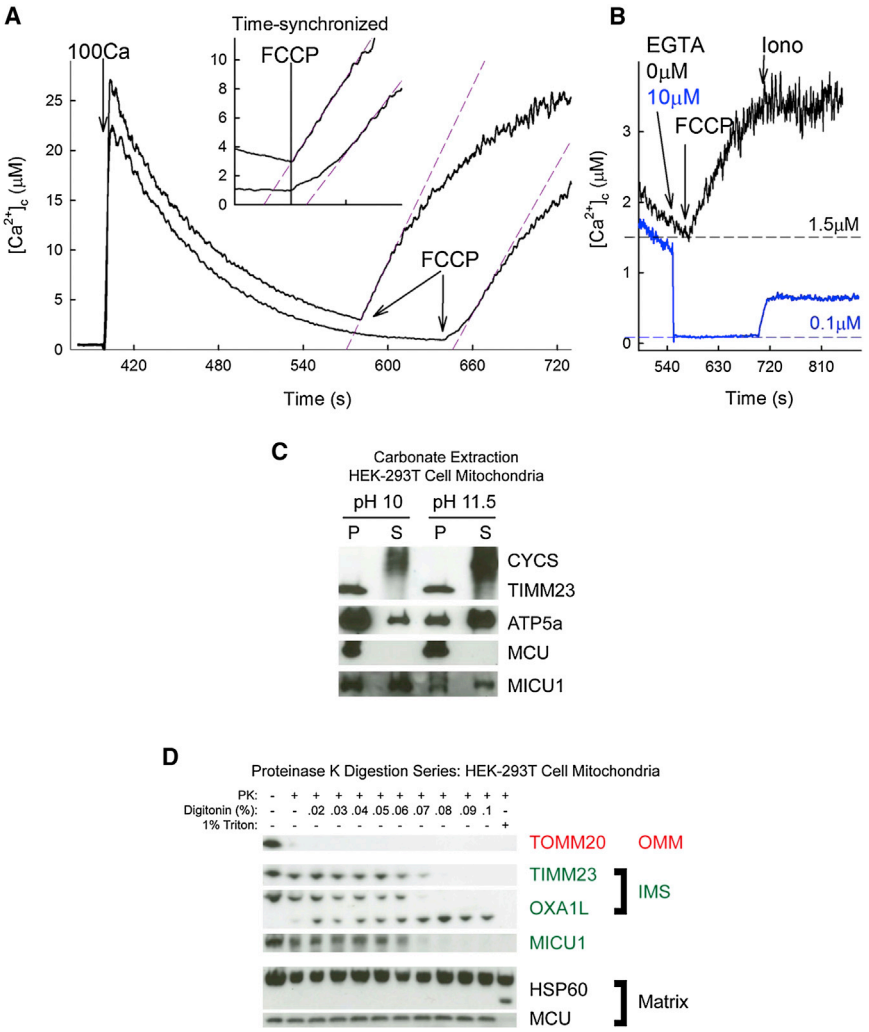

Figure 4. MICU1 Faces the Outer Surface of the IMM to Sense $[Ca^{2+}]_c$

(A) Representative $[Ca^{2+}]_c$ time courses of the mitochondrial clearance of a 100 μM $CaCl_2$ pulse and the subsequent FCCP-induced Ca^{2+} release (as in Figure 3C). FCCP is added at different time points during the $[Ca^{2+}]_c$ recovery phase. Linear fits are laid over the fast phase of Ca^{2+} release (purple dashed lines) to underscore the differences in the initial kinetics. In the inset the two FCCP additions are time synchronized to further emphasize $[Ca^{2+}]_c$ dependence (90 s time period is shown).

(B) One hundred fifty seconds after addition of a 10 μM $CaCl_2$ pulse, either 0 (black) or 10 μM (blue) EGTA was added to establish different $[Ca^{2+}]_c$. Without EGTA addition, FCCP fully released the mitochondria-accumulated Ca^{2+} in 2 min (no further $[Ca^{2+}]_c$ increase upon addition of Ca^{2+} ionophore ionomycin). Lowering $[Ca^{2+}]_c$ to 0.1 μM by EGTA abolished the $[Ca^{2+}]_c$ increase caused by FCCP, but subsequent ionomycin addition caused substantial $[Ca^{2+}]_c$ increase, indicating the continued accumulation of Ca^{2+} in the mitochondria.

(C and D) Topology of MICU1 was investigated using isolated HEK293T cell mitochondria. (C) Analysis of supernatant (S) and insoluble pellet (P) fractions following carbonate extraction at pH 10 and pH 11.5 with immunoblotting against MICU1 and the established integral membrane proteins TIMM23 and MCU, the soluble protein CYCS, and the peripheral membrane protein ATP5a. (D) Mitochondria were treated with PK with increasing concentrations of detergent. Proteins with known localization are immunoblotted and labeled according to their topology. Bands representing cleavage products are shown for OXA1L and HSP60 (with Triton).

MICU1 Is Localized at the Outer Surface of the IMM to Sense $[Ca^{2+}]_c$

In Ctrl cells, when Ca^{2+} efflux was initiated at lower $[Ca^{2+}]_c$, a slow-onset and biphasic $[Ca^{2+}]_c$ rise occurred (Figure 4A). However, when FCCP was added before $[Ca^{2+}]_c$ had returned to $\leq$1 μM, the $[Ca^{2+}]_c$ rise started steeply, without delay (Figure 4A). The initial rate of the $[Ca^{2+}]_c$ rise progressively increased with $[Ca^{2+}]_c$ (Figure S3C). Higher $[Ca^{2+}]_c$ at the point of FCCP addition equates to less Ca^{2+} having been taken up by the mitochondria, and therefore the faster release could not be driven by a greater $[Ca^{2+}]$ gradient. The $[Ca^{2+}]_c$ requirement for facilitating the mtCU-mediated Ca^{2+} efflux was further supported by the observation that lowering of $[Ca^{2+}]_c$ to 100 nM prevented the FCCP-induced Ca^{2+} efflux (Figure 4B). Thus, activation of the Ca^{2+} flux through mtCU is positively regulated by $[Ca^{2+}]_c$. Considering that neither the activation of mtCU by $[Ca^{2+}]_c$ nor the MICU1 dependence (Figures 3C and 3D) seems to be eliminated by a large increase in matrix Ca^{2+}, the Ca^{2+} sensing site(s) of MICU1 is likely present in the IMS rather than the matrix.

Given the functional evidence to support an IMS localization of the calcium sensing site(s) of MICU1, we sought to corroborate with biochemical evidence. To this end, we examined the topology of MICU1, including both the nature of membrane association and the submitochondrial localization. An alkaline carbonate extraction of isolated HEK293T cell mitochondria reveals that MICU1 is likely strongly associated with the IMM (Figure 4C): MICU1 is observed in both supernatant and pellet fractions at both pH 10 and pH 11.5 following carbonate extraction. Integral membrane proteins such as TIMM23 and MCU, on the other hand, remain only in the pellet under either condition. In order to determine the submitochondrial localization of MICU1, we further used a Proteinase K (PK) digestion with a series of detergent concentrations to differentially permeabilize the IMM and OMM in HEK293T cell mitochondria (Figure 4D). MICU1 is protected from proteolysis similarly to the IMS proteins TIMM23 and OXA1L, whereas the matrix proteins HSP60 and MCU do not get digested until the end of the series. All proteins shown, however, are substrates for PK as evidenced by digestion in 1% Triton X-100. Collectively, these results provide both biochemical and functional evidence that MICU1 and its Ca^{2+} sensing site are exposed to $[Ca^{2+}]_c$ at the outer surface of the IMM.

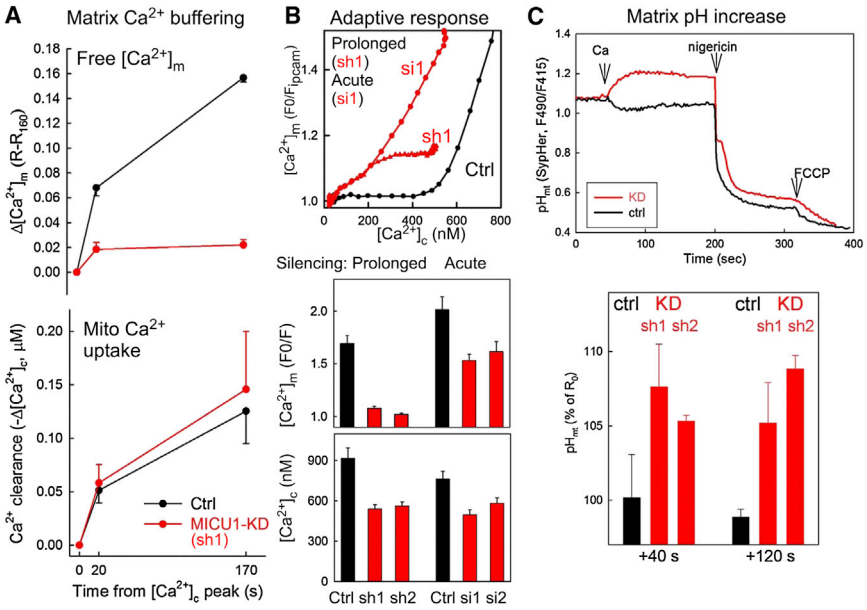

Figure 5. Enhanced Mitochondrial Matrix Ca^{2+} Chelation as an Adaptive Response to MICU1 Depletion

(A) Mitochondrial Ca^{2+} uptake (lower) and the corresponding increase in $[Ca^{2+}]_m$ (upper) were monitored simultaneously in permeabilized HeLa cells in the presence of Tg. To obtain comparable Ca^{2+} uptake, 5 μM and 2 μM $CaCl_2$ were added to Ctrl and stable MICU1-KD cells, respectively (n = 4).

(B) (Top) $[Ca^{2+}]_m$ versus $[Ca^{2+}]_c$ relationships during SOCE in acute (48 hr, si1) and stable MICU1-KD (sh1,2) cells. Middle and lower graphs show the peak $[Ca^{2+}]_m$ and $[Ca^{2+}]_c$ increases evoked by SOCE (1 mM $CaCl_2$) (n = 24–62).

(C) Mitochondrial matrix alkalinization in stable MICU1-KD (sh1 and sh2) cells during SOCE (1 mM $CaCl_2$) recorded by mtSypHer. Ionophore (Nigericin, 5 μM) and FCCP (5 μM) were added to induce matrix acidification. Representative traces (upper) and mean normalized post-SOCE (40 and 120 s) values (lower n = 3–4, $p < 0.05$).

Enhanced Mitochondrial Matrix Ca^{2+} Chelation as an Adaptive Response to MICU1 Depletion

We next explored the blunted $[Ca^{2+}]_m$ rise in MICU1-KD cells. A decrease in the cooperativity of mtCU's activation might be a factor in the blunted $[Ca^{2+}]_m$ increases elicited by short-lasting $[Ca^{2+}]_c$ microdomains during IP_3-linked stimulation. However, it is unlikely to fully account for the suppression of the $[Ca^{2+}]_m$ signal during the sustained SOCE (Figures 1E–1G). Also, Figures 1J–1L showed that the attenuated $[Ca^{2+}]_m$ increase was associated with enhanced Ca^{2+} sequestration. The combination of enhanced Ca^{2+} storage and an attenuated $[Ca^{2+}]_m$ rise indicates that an increased fraction of Ca^{2+} was in bound form in the mitochondrial matrix of stable MICU1-KD. To directly test this possibility, simultaneous quantification of mitochondrial Ca^{2+} accumulation and the corresponding $[Ca^{2+}]_m$ increase was set up in permeabilized cells (Figure 5A). During continuous mitochondrial Ca^{2+} uptake, the $[Ca^{2+}]_m$ showed a progressive increase in Ctrl but only a small $[Ca^{2+}]_m$ increase in MICU1-KD (Figure 5A). This result indicates that much of the accumulated Ca^{2+} is in bound form, suggesting increased matrix Ca^{2+} buffering capacity.

To test if the change in matrix Ca^{2+} buffering is directly linked to MICU1 depletion, Ca^{2+} transport was also monitored during short-term (48 hr) silencing (si1 in Figure 5B). MICU1 depletion upon short-term silencing was similar to that in the stable cell lines (data not shown). Both short- and long-term depletion of MICU1 caused a similar decrease in the $[Ca^{2+}]_c$ threshold for the $[Ca^{2+}]_m$ rise, but suppression of the amplitude of the $[Ca^{2+}]_m$ response was not induced by acute MICU1 silencing (Figure 5B). Thus, upregulation of the matrix Ca^{2+} buffering may be an adaptive response to prolonged MICU1 depletion.

Mitochondrial matrix pH (pH_m) is central to matrix Ca^{2+} buffering (Chalmers and Nicholls, 2003). Measurement of pH_m by a genetically targeted reporter, mtSypHer (Poburko et al., 2011), revealed alkalinization in stable MICU1-KD cells during mitochondrial Ca^{2+} uptake (Figure 5C), whereas no change or a slight acidification was observed in the Ctrl, in agreement with a previous study (Poburko et al., 2011).

Collectively, these results suggest that prolonged MICU1 depletion may lead to an adaptive increase in mitochondrial matrix Ca^{2+} binding, which may be linked to pH_m. Upregulation of matrix Ca^{2+} buffering provides an explanation for the blunted $[Ca^{2+}]_m$ increases during $[Ca^{2+}]_c$ signaling events in long-term silenced HeLa cells.

Increased Sensitivity of MICU1-KD Cells to Delayed Mitochondrial Ca^{2+} Dysregulation: Role of ROS

An increase in mitochondrial Ca^{2+} storage has been linked to delayed mitochondrial dysregulation, membrane permeabilization, and cell injury (Chalmers and Nicholls, 2003). Continuous mitochondrial Ca^{2+} loading in conjunction with other stress factors triggers loss of IMM integrity, which manifests as dissipation of $\Delta\Psi_m$ and release of Ca^{2+} (Csordás et al., 2006; Pacher and Hajnóczky, 2001). When prolonged SOCE was stimulated in HeLa cells (Figure S4A) or hepatocytes (Figure S4C), MICU1-KD cells showed a greatly enhanced vulnerability to $\Delta\Psi_m$ loss. The impairment of mitochondria was followed by an increase in cell death (Figure S4B).

Enhanced production of reactive oxygen species (ROS) might contribute to the mitochondrial injury, since Ca^{2+} stimulates ROS production and ROS is known to synergize with Ca^{2+} to induce mitochondrial membrane permeabilization. Using mtHyPer, an H_2O_2 reporter genetically targeted to the mitochondrial matrix (Belousov et al., 2006), no change in resting H_2O_2 was observed in association with MICU1 depletion (Figure S4D, left panel). However, during prolonged SOCE a gradual increase in matrix H_2O_2 was detected in MICU1-KD (Figure S4D, right panel), which might make some contribution in mitochondrial membrane permeabilization.

These results show that loss of MICU1 causes vulnerability of mitochondria to stress, leading to impaired cellular function. The impairments involve stress-related enhanced ROS generation.

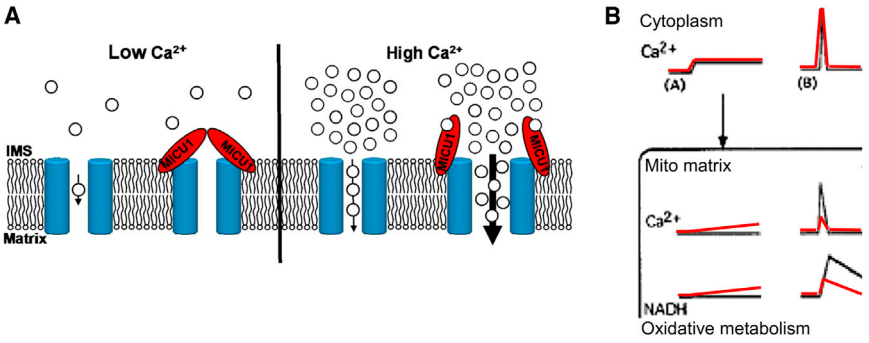

Figure 6. MICU1 Supports Decoding of $[Ca^{2+}]_c$ Signals by Stabilizing the Closed State and Supporting Ca^{2+}-Dependent Activation of mtCU

(A) Graphical representation of the modulation of mtCU by MICU1.

(B) The model depicts the two major flaws in mitochondrial $[Ca^{2+}]_c$ signal detection and the coupled Ca^{2+} control of oxidative metabolism in MICU1-deficient cells. Small $[Ca^{2+}]_c$ elevations (A) are tuned out by Ctrl (black) mitochondria owing to MICU1-dependent thresholding but are able to propagate to the MICU1-deficient (red) mitochondria, causing stimulation and long-term exhaustion of oxidative metabolism. Large $[Ca^{2+}]_c$ transients (B) such as the rapid short-lasting IP3R-derived high $[Ca^{2+}]_c$ microdomains are effectively transferred to the mitochondrial matrix due to MICU1-dependent cooperative activation of mtCU. In the absence of MICU1, the efficacy of signal propagation decreases. Please note that oxidative metabolism was assessed by NAD(P)H imaging in Hajnóczky et al. (1995) and by cellular JO2 measurement in the present study.

Thus, the physiological roles of MICU1 might be to prevent mitochondrial Ca^{2+} overload at moderate $[Ca^{2+}]_c$ elevations and to allow optimal $[Ca^{2+}]_m$ and metabolic responses to $[Ca^{2+}]_c$ spikes.

Role of MICU1 in Decoding of Cytoplasmic Calcium Signals by the Mitochondria

Taken together, our data lead us to construct the model of mtCU regulation by MICU1 illustrated in Figure 6A. MICU1 localizes to the outer surface of the IMM, as evidenced by Figures 6C and 6D, and presents a site for regulation of mtCU by $[Ca^{2+}]_c$. In this model, MICU1 contributes to keeping mtCU closed at low $[Ca^{2+}]_c$. At high $[Ca^{2+}]_c$, MICU1 promotes activation of the channel. Therefore, MICU1 can be envisioned as a Ca^{2+}-sensitive switch supporting effective transitions of mtCU between closed and open states.

How do the effects of MICU1 on mtCU activity contribute to the decoding of calcium spikes and oscillations? Figures 1E, 1G, and 1H have already shown that submicromolar $[Ca^{2+}]_c$ increases can reach the mitochondrial matrix only in MICU1-KD cells. Thus, MICU1 helps mitochondria to tune out $[Ca^{2+}]_c$ baseline fluctuations. Figures 1B and 1C and Figure S1D also showed suppression of the IP_3-linked $[Ca^{2+}]_m$ transients in hepatocytes. This could be because mitochondrial Ca^{2+} uptake was less efficient in MICU1-KD but local $[Ca^{2+}]_c$ transients sensed by mitochondria or Ca^{2+} binding in the mitochondrial matrix could also be affected by MICU1 KD. To discriminate among these possibilities, first local $[Ca^{2+}]$ at the ER-mitochondrial interface was directly monitored (Csordás et al., 2010), and no difference was found between MICU1-KD and Ctrl (Figure S5A). Then the effects on $[Ca^{2+}]_m$ of IP_3-linked stimulation and SOCE were tested in side-by-side measurements. The IP3R-mediated local high $[Ca^{2+}]$ could evoke only a slowly developing $[Ca^{2+}]_m$ increase in MICU1-KD compared to Ctrl (Figure S5B). Furthermore, when $[Ca^{2+}]_m$ was recorded simultaneously with and plotted against the local $[Ca^{2+}]_c$ at the mitochondrial surface (Figure S5C), unlike the Ctrl (left), the MICU1-KD (right) failed to show steeper correlation upon histamine stimulation (continuous line) than during SOCE (dashed line). Differential suppression of the histamine-induced $[Ca^{2+}]_m$ increase in MICU1-KD cannot be explained by an increase in mitochondrial matrix Ca^{2+} chelation. These results further indicate that MICU1 is specifically required for the steep activation of the uniporter and mitochondrial Ca^{2+} uptake during short-lasting IP3R-mediated $[Ca^{2+}]_c$ signals. Thus MICU1 provides a Ca^{2+}-dependent molecular switch that allows mitochondrial decoding of the $[Ca^{2+}]_c$ signal, specifically both the exclusion of slow and small $[Ca^{2+}]_c$ increases and the positive selection of IP3R-mediated $[Ca^{2+}]_c$ spikes to propagate to the mitochondrial matrix via mtCU. To highlight the function of MICU1, the scheme in Figure 6B shows a previously suggested adaptation of the descriptive model linking cytoplasmic and mitochondrial Ca^{2+} signals to metabolism (Hajnóczky et al., 1995). The original figure, representing the control condition, is shown in black with the alterations occurring in the absence of MICU1 shown in red.

DISCUSSION

Our findings show that MICU1 has two distinct functions in the regulation of the mtCU: (1) it sets a $[Ca^{2+}]_c$ threshold ($\geq$500 nM), and (2) it provides cooperative activation as $[Ca^{2+}]_c$ rises. As a result, MICU1 enables mitochondria to tune out small and slow $[Ca^{2+}]_c$ increases, avoiding chronic, superfluous stimulation, while responding effectively to large and rapid $[Ca^{2+}]_c$ spikes and oscillations during periods of activity (see schematic in Figure 6B). Because MICU1 lacking functional Ca^{2+}-binding EF-hands is able to threshold Ca^{2+} uniport at low $[Ca^{2+}]_c$ as wild-type MICU1, but cannot confer cooperative activation as $[Ca^{2+}]_c$ rises, the steep transition between fully closed and open states of MCU must be mediated by binding of Ca^{2+} to MICU1's EF-hands. As MICU1 and MCU reside within the same macromolecular complex, we propose that Ca^{2+} binding to MICU1 induces a conformational change that is relayed to the pore, positively regulating the uniporter activity (Figure 6A).

In a recent paper, Mallilankaraman et al. also described the thresholding function of MICU1; however, they did not observe a role of MICU1 in controlling mtCU cooperativity. Thus, both studies agree that a key role for MICU1 is to keep mtCU closed. In the high $[Ca^{2+}]_c$ range, the role of MICU1 in the allosteric control of mtCU may have been missed previously because the transport assay was performed in the absence of physiological $[Mg^{2+}]$ (Mallilankaraman et al., 2012b). Previous studies have shown that Mg^{2+} controls the allosteric activation of the uniporter (Bragadin et al., 1979; Favaron and Bernardi, 1985; Kröner,

1986), and we demonstrate here that Mg^{2+} is needed to support the effect of MICU1 on mtCU cooperativity (Figure S3).

Our results show that resting $[Ca^{2+}]_m$ is unaltered in MICU1-KD cells, but the IP3R-mediated increase of $[Ca^{2+}]_m$ is suppressed (Figure 1). Previously, Perocchi et al. described suppression of both resting and stimulated $[Ca^{2+}]_m$ levels in HeLa cells (Perocchi et al., 2010), and Mallilankaraman et al. reported an elevation of the resting $[Ca^{2+}]_m$ but no change in the IP3R-mediated increase (Mallilankaraman et al., 2012b). The reasons for the differences appear to be at least in part technical. Mallilankaraman et al. used a nonratiometric dye-based assay (rhod2) to record $[Ca^{2+}]_m$ without calibration or confirmation of dye distribution. This way, fluorescence intensity values may not equate to Ca^{2+} concentrations. MCU or MICU1 silencing may also change rhod2 accumulation to the mitochondria and in other organelles. To avoid these problems, we used genetically targeted Ca^{2+} sensors, as did Perocchi et al. However, these probes can be influenced by pH, and we have documented alkalinization in the mitochondrial matrix during SOCE in MICU1-KD (Figure 5). Therefore, we used multiple probes, including ratiometric pericam that is pH insensitive when excited at 415 nm (Jiang et al., 2009) (Figure 1). Moreover, we estimated the resting mitochondrial Ca^{2+} by monitoring $[Ca^{2+}]_c$ increase caused by uncoupling in intact cells (Figure S1). All these results suggest that in MICU1-KD cells, mitochondria do not take up Ca^{2+} at the resting $[Ca^{2+}]_c$ which is set by high-affinity plasma membrane and ER Ca^{2+} pumps ($\leq$100 nM). However, when Ca^{2+} pumps are disabled, mitochondria establish a steady state of $[Ca^{2+}]_c$ <300 nM in MICU1-KD (Figure 2C). Therefore a possible explanation for any elevated basal $[Ca^{2+}]_m$ by Mallilankaraman et al. can be that the resting $[Ca^{2+}]_c$ was somewhat higher or the Ca^{2+} pumps were less active in their model.

The attenuated IP3R-mediated $[Ca^{2+}]_m$ increase likely reflects decreased uptake in response to the high $[Ca^{2+}]_c$ microdomains due to lessened cooperativity in mtCU activation. Furthermore, we have shown that depletion of MICU1 induces adaptive responses that include an increase in the bound fraction of total mitochondrial calcium (Figure 5). This adaptation is more apparent in stable (long-term) than in short-term silencing (Figure 5B). Notably, we also observed some increase in the exchanger-mediated mitochondrial Ca^{2+} efflux in stable MICU1-KD (data not shown), which may contribute to lowering the mitochondrial Ca^{2+} load. Thus, model-specific differences in the compensatory responses might also contribute to the variability in suppression of the $[Ca^{2+}]_m$ signal shown in the three studies.

Mitochondria in most tissues and cell types effectively respond to $[Ca^{2+}]_c$ spikes and oscillations that involve elevation of the global $[Ca^{2+}]_c$ to ~1 μM. This has been attributed to strategic localization of mitochondria close to Ca^{2+} release channels of the ER/SR (Csordás et al., 1999; Hajnóczky et al., 1995; Lawrie et al., 1996; Rizzuto et al., 1993; Rizzuto et al., 1998), because these mitochondria are exposed to local $[Ca^{2+}]$ rises attaining 5–10 μM (Csordás et al., 2010; Giacomello et al., 2010). However, these local $[Ca^{2+}]$ increases are usually short-lasting. Therefore, it is central to the mitochondrial sensing of the $[Ca^{2+}]_c$ spikes that mitochondrial Ca^{2+} uptake is rapidly and steeply activated in the micromolar range of $[Ca^{2+}]_c$. Indeed, a regulatory Ca^{2+}-binding site has already been proposed (Csordás and Hajnóczky, 2003; Gunter and Pfeiffer, 1990; Kröner, 1986). However, the Ca^{2+} sensor remained elusive. Here, we demonstrated that the cooperative activation of mtCU is suppressed in cells lacking MICU1 or expressing MICU1 mutated at both Ca^{2+} binding EF-hand domains. Thus, MICU1 represents a molecular switch that binds Ca^{2+} to sharply enhance mtCU-mediated Ca^{2+} influx in the micromolar $[Ca^{2+}]_c$ range.

Previously, patch-clamp studies demonstrated that I_{MiCa} amplitude was not noticeably altered when pipette (intramitoplast) $[Ca^{2+}]$ was varied from <10 nM to about 10 μM (Kirichok et al., 2004). Furthermore, our results demonstrated that preloading of mitochondria with Ca^{2+} (1) did not affect the biphasic kinetic of mtCU-mediated Ca^{2+} flux (Figure 4A) and (2) did not attenuate the MICU1-dependent difference in the Ca^{2+} flux if submicromolar $[Ca^{2+}]_c$ was restored (Figure 3). We further show biochemical evidence that MICU1 faces the IMS, and not the matrix as previously reported (Mallilankaraman et al., 2012b), and probably its EF-hands form the proposed allosteric Ca^{2+} regulatory site of mtCU in the IMS (Igbavboa and Pfeiffer, 1988).

Mitochondria isolated from various tissues and in a wide range of cell lines display minimal Ca^{2+} uptake in the physiological range of global $[Ca^{2+}]_c$ (Gunter et al., 1994), though higher-affinity mitochondrial Ca^{2+} uptake has been documented in some hormone-producing cell types and cardiac muscle (Sparagna et al., 1995; Spät et al., 2008). Similar to most tissues and cell types, in primary hepatocytes and HeLa cells, mitochondrial Ca^{2+} uptake is noticeable only in the micromolar $[Ca^{2+}]_c$ range, and a $[Ca^{2+}]_m$ increase requires $\geq$500 nM $[Ca^{2+}]_c$ in practically every cell (Figure 1). By contrast, in MICU1-deficient cells mitochondrial Ca^{2+} uptake is detectable below 300 nM of $[Ca^{2+}]_c$ (Figures 1 and 2). This difference does not seem to have much effect on mitochondrial Ca^{2+} handling when $[Ca^{2+}]_c$ is maintained at the resting level (<100 nM) by the activity of the high-affinity plasma membrane and ER Ca^{2+} pumps. However, submicromolar $[Ca^{2+}]_c$ fluctuations that are normally ignored by the mitochondria in plain cells are routed to the mitochondria if MICU1 expression is decreased. Thus physiological changes in global $[Ca^{2+}]_c$ that are handled mostly by the plasma membrane and ER Ca^{2+} pumps in normal cells are shifted toward mitochondria if MICU1 is not expressed at normal levels.

MICU1 resides in a complex with MCU, which is hypothesized to be the pore-forming component of mtCU, since it is sufficient by itself to provide a current in planar bilayers similar to I_{MiCa} (Baughman et al., 2011; De Stefani et al., 2011; Kirichok et al., 2004). At present we do not know whether MICU1 impacts the ion selectivity of mtCU. Our data indicate that MICU1 without bound Ca^{2+} helps to keep the gate closed at submicromolar $[Ca^{2+}]_c$. At higher $[Ca^{2+}]_c$, mtCU activity increases even without MICU1 or if the EF-hands are mutated, but a much steeper activation is seen with native MICU1. These results are in line with earlier observations that the open probability for I_{MiCa} in mitoplasts, where MICU1 is expected to be present, is much higher than that of the reconstituted MCU channel in lipid bilayer under comparable electrical (−160 mV) and $[Ca^{2+}]$ (symmetrical ~100 mM) conditions (De Stefani et al., 2011; Kirichok et al., 2004). Our prediction, then, is that binding of Ca^{2+} to MICU1 results in a conformational change sensed by the MCU and translated to positive cooperative gating of the channel by Ca^{2+}. Many

ion channels of the plasma membrane or ER/SR are regulated by Ca^{2+} binding. In most cases the pore-forming component of the channel contains a Ca^{2+} binding site(s) (e.g., L-type voltage-gated Ca^{2+} channels, BK channels, TRPV5/6, IP3R, RyR). However, in some cases a separate Ca^{2+} sensing protein is employed to control the gate, such as calmodulin for the SK potassium channels and STIM1 for ORAI. Perhaps the closest analog to our model of mtCU is the SK channel, where calmodulin is permanently associated with the pore and upon binding of Ca^{2+} triggers the opening of the gate (Fakler and Adelman, 2008).

The current study proposes a simple model that combines the Ca^{2+}-sensing activity of MICU1 and the pore-forming subunit MCU (Figure 6); however, the mechanisms controlling mtCU dynamics are likely to be more complicated. While our experiments were performed in HeLa cells and in some cases hepatocytes as well, we anticipate variation across cell and tissue types. MICU2, a paralog of MICU1, resides within the MICU1/MCU complex (Plovanich et al., 2013). MCU itself has a paralog, CCDC109b, whose function is still not clear. Several other regulators, including MCUR1 (Mallilankaraman et al., 2012a), have been identified that may interact more indirectly. We anticipate that the relationship between MICU1/2 and MCU is particularly intimate, given the striking coevolution of these proteins (Baughman et al., 2011; Bick et al., 2012), their strong coexpression (Baughman et al., 2011), and their genomic adjacency (Bick et al., 2012).

Decoding of $[Ca^{2+}]_c$ spikes and oscillations by mtCU was shown to be central to cytoplasmic Ca^{2+} signaling (Hajnóczky et al., 1999; Jouaville et al., 1995; Tinel et al., 1999), to control of oxidative metabolism (Hajnóczky et al., 1995; Jouaville et al., 1999; Robb-Gaspers et al., 1998), and even to induction of apoptosis under conditions of cellular stress (Szalai et al., 1999). All these functions of mtCU are severely disturbed when MICU1 is depleted. Sensitization of mtCU to $[Ca^{2+}]_c$ results in mitochondrial suppression of both Ca^{2+} entry and IP3R-dependent fluctuations in global $[Ca^{2+}]_c$. Attenuation of the agonist-induced $[Ca^{2+}]_m$ elevations leads to weakened activation of the matrix dehydrogenases (Perocchi et al., 2010). The observed dysregulation of respiration in the MICU1-depleted cells is also likely caused by the altered mitochondrial Ca^{2+} handling. Finally, the impairment of bioenergetics makes the cells vulnerable to various stress factors, increasing the risk for cell death. Thus, the MICU1-dependent control over the $[Ca^{2+}]_c$ thresholding and cooperativity of mtCU is critical for effective cytoplasmic and mitochondrial calcium signaling and, in turn, for cell survival.

EXPERIMENTAL PROCEDURES

Detailed protocols are listed in the Supplemental Experimental Procedures.

DNA Constructs and Transient Expression

See the Supplemental Information.

Silencing of MICU1 or MCU

In vivo silencing in mouse liver was applied for 4 weeks as described previously (Baughman et al., 2011). Studies were done in accordance with the institutional review board guidelines. Stable expression of shRNAs and wild-type and mutant proteins has been described (Baughman et al., 2011; Perocchi et al., 2010). For short-term silencing, HeLa cells were transfected with the siRNA version of the same sh1 and sh2 hairpins used for stable cells (Ambion) or with scrambled siRNA for 48 hr using Oligofectamine (Invitrogen).

Live-Cell Imaging and Fluorometric Measurements

Live-cell imaging and fluorometric measurements of $[Ca^{2+}]_c$, $[Ca^{2+}]_m$, and $\Delta\Psi_m$, respectively, were performed as described earlier (Csordás and Hajnóczky, 2003; Csordás et al., 2010). pH_m was measured with mtSypHer (Poburko et al., 2011). For SOCE experiments ER stores were depleted by 10 min pretreatment with 2 μM Tg in Ca^{2+}-free buffer.

MICU1 Topology Analysis

Localization analysis and alkaline carbonate extraction were performed using HEK293T mitochondria according to Sato and Mihara (2010) and Ryan et al. (2001), respectively.

Measurement of Cellular Oxygen Consumption

JO_2 was measured using an XF24 Extracellular Flux analyzer (Seahorse Biosciences) at 37°C.

Statistics

Experiments were carried out with three or more different cell preparations and with each at least in triplicate. Data are presented as mean ± SE. Significance of differences from the relevant controls was calculated by Student's t test or Tukey post hoc test following two-way ANOVA. Modeling is described in the Supplemental Information.

SUPPLEMENTAL INFORMATION

Supplemental Information includes five figures, Supplemental Experimental Procedures, and Supplemental References and can be found with this article online at http://dx.doi.org/10.1016/j.cmet.2013.04.020.

ACKNOWLEDGMENTS

We thank Olga Goldberger for technical assistance, and B.R. Bettencourt, K. Charisse, S. Kuchimanchi, and A. Akinc of Alnylam Pharmaceuticals for siRNA design, synthesis, and formulation. This work was supported by NIH grants DK080261 (to V.K.M.) and DK051526 (to G.H.). V.K. was formerly an employee at and received compensation from Alnylam Pharmaceuticals.

Received: February 3, 2012
Revised: April 2, 2013
Accepted: April 26, 2013
Published: June 4, 2013

REFERENCES

Baughman, J.M., Perocchi, F., Girgis, H.S., Plovanich, M., Belcher-Timme, C.A., Sancak, Y., Bao, X.R., Strittmatter, L., Goldberger, O., Bogorad, R.L., et al. (2011). Integrative genomics identifies MCU as an essential component of the mitochondrial calcium uniporter. Nature *476*, 341–345.

Belousov, V.V., Fradkov, A.F., Lukyanov, K.A., Staroverov, D.B., Shakhbazov, K.S., Terskikh, A.V., and Lukyanov, S. (2006). Genetically encoded fluorescent indicator for intracellular hydrogen peroxide. Nat. Methods *3*, 281–286.

Beutner, G., Sharma, V.K., Lin, L., Ryu, S.Y., Dirksen, R.T., and Sheu, S.S. (2005). Type 1 ryanodine receptor in cardiac mitochondria: transducer of excitation-metabolism coupling. Biochim. Biophys. Acta *1717*, 1–10.

Bick, A.G., Calvo, S.E., and Mootha, V.K. (2012). Evolutionary diversity of the mitochondrial calcium uniporter. Science *336*, 886.

Bragadin, M., Pozzan, T., and Azzone, G.F. (1979). Kinetics of Ca2+ carrier in rat liver mitochondria. Biochemistry *18*, 5972–5978.

Chalmers, S., and Nicholls, D.G. (2003). The relationship between free and total calcium concentrations in the matrix of liver and brain mitochondria. J. Biol. Chem. *278*, 19062–19070.

Csordás, G., and Hajnóczky, G. (2003). Plasticity of mitochondrial calcium signaling. J. Biol. Chem. *278*, 42273–42282.

Csordás, G., Thomas, A.P., and Hajnóczky, G. (1999). Quasi-synaptic calcium signal transmission between endoplasmic reticulum and mitochondria. EMBO J. *18*, 96–108.

Csordás, G., Renken, C., Várnai, P., Walter, L., Weaver, D., Buttle, K.F., Balla, T., Mannella, C.A., and Hajnóczky, G. (2006). Structural and functional features and significance of the physical linkage between ER and mitochondria. J. Cell Biol. *174*, 915–921.

Csordás, G., Várnai, P., Golenár, T., Roy, S., Purkins, G., Schneider, T.G., Balla, T., and Hajnóczky, G. (2010). Imaging interorganelle contacts and local calcium dynamics at the ER-mitochondrial interface. Mol. Cell *39*, 121–132.

de Brito, O.M., and Scorrano, L. (2008). Mitofusin 2 tethers endoplasmic reticulum to mitochondria. Nature *456*, 605–610.

De Stefani, D., Raffaello, A., Teardo, E., Szabò, I., and Rizzuto, R. (2011). A forty-kilodalton protein of the inner membrane is the mitochondrial calcium uniporter. Nature *476*, 336–340.

Fakler, B., and Adelman, J.P. (2008). Control of K(Ca) channels by calcium nano/microdomains. Neuron *59*, 873–881.

Favaron, M., and Bernardi, P. (1985). Tissue-specific modulation of the mitochondrial calcium uniporter by magnesium ions. FEBS Lett. *183*, 260–264.

Giacomello, M., Drago, I., Bortolozzi, M., Scorzeto, M., Gianelle, A., Pizzo, P., and Pozzan, T. (2010). Ca2+ hot spots on the mitochondrial surface are generated by Ca2+ mobilization from stores, but not by activation of store-operated Ca2+ channels. Mol. Cell *38*, 280–290.

Gunter, T.E., and Pfeiffer, D.R. (1990). Mechanisms by which mitochondria transport calcium. Am. J. Physiol. *258*, C755–C786.

Gunter, T.E., Gunter, K.K., Sheu, S.S., and Gavin, C.E. (1994). Mitochondrial calcium transport: physiological and pathological relevance. Am. J. Physiol. *267*, C313–C339.

Hajnóczky, G., Robb-Gaspers, L.D., Seitz, M.B., and Thomas, A.P. (1995). Decoding of cytosolic calcium oscillations in the mitochondria. Cell *82*, 415–424.

Hajnóczky, G., Hager, R., and Thomas, A.P. (1999). Mitochondria suppress local feedback activation of inositol 1,4, 5-trisphosphate receptors by Ca2+. J. Biol. Chem. *274*, 14157–14162.

Igbavboa, U., and Pfeiffer, D.R. (1988). EGTA inhibits reverse uniport-dependent Ca2+ release from uncoupled mitochondria. Possible regulation of the Ca2+ uniporter by a Ca2+ binding site on the cytoplasmic side of the inner membrane. J. Biol. Chem. *263*, 1405–1412.

Jiang, D., Zhao, L., and Clapham, D.E. (2009). Genome-wide RNAi screen identifies Letm1 as a mitochondrial Ca2+/H+ antiporter. Science *326*, 144–147.

Jouaville, L.S., Ichas, F., Holmuhamedov, E.L., Camacho, P., and Lechleiter, J.D. (1995). Synchronization of calcium waves by mitochondrial substrates in Xenopus laevis oocytes. Nature *377*, 438–441.

Jouaville, L.S., Pinton, P., Bastianutto, C., Rutter, G.A., and Rizzuto, R. (1999). Regulation of mitochondrial ATP synthesis by calcium: evidence for a long-term metabolic priming. Proc. Natl. Acad. Sci. USA *96*, 13807–13812.

Kirichok, Y., Krapivinsky, G., and Clapham, D.E. (2004). The mitochondrial calcium uniporter is a highly selective ion channel. Nature *427*, 360–364.

Kröner, H. (1986). ''Allosteric regulation'' of calcium-uptake in rat liver mitochondria. Biol. Chem. Hoppe Seyler *367*, 483–493.

Lawrie, A.M., Rizzuto, R., Pozzan, T., and Simpson, A.W. (1996). A role for calcium influx in the regulation of mitochondrial calcium in endothelial cells. J. Biol. Chem. *271*, 10753–10759.

Mallilankaraman, K., Cárdenas, C., Doonan, P.J., Chandramoorthy, H.C., Irrinki, K.M., Golenár, T., Csordás, G., Madireddi, P., Yang, J., Müller, M., et al. (2012a). MCUR1 is an essential component of mitochondrial Ca2+ uptake that regulates cellular metabolism. Nat. Cell Biol. *14*, 1336–1343.

Mallilankaraman, K., Doonan, P., Cárdenas, C., Chandramoorthy, H.C., Müller, M., Miller, R., Hoffman, N.E., Gandhirajan, R.K., Molgó, J., Birnbaum, M.J., et al. (2012b). MICU1 is an essential gatekeeper for MCU-mediated mitochondrial Ca(2+) uptake that regulates cell survival. Cell *151*, 630–644.

Marchant, J.S., Ramos, V., and Parker, I. (2002). Structural and functional relationships between Ca2+ puffs and mitochondria in Xenopus oocytes. Am. J. Physiol. Cell Physiol. *282*, C1374–C1386.

Pacher, P., and Hajnóczky, G. (2001). Propagation of the apoptotic signal by mitochondrial waves. EMBO J. *20*, 4107–4121.

Pacher, P., Thomas, A.P., and Hajnóczky, G. (2002). Ca2+ marks: miniature calcium signals in single mitochondria driven by ryanodine receptors. Proc. Natl. Acad. Sci. USA *99*, 2380–2385.

Perocchi, F., Gohil, V.M., Girgis, H.S., Bao, X.R., McCombs, J.E., Palmer, A.E., and Mootha, V.K. (2010). MICU1 encodes a mitochondrial EF hand protein required for Ca(2+) uptake. Nature *467*, 291–296.

Pinton, P., Ferrari, D., Rapizzi, E., Di Virgilio, F., Pozzan, T., and Rizzuto, R. (2001). The Ca2+ concentration of the endoplasmic reticulum is a key determinant of ceramide-induced apoptosis: significance for the molecular mechanism of Bcl-2 action. EMBO J. *20*, 2690–2701.

Plovanich, M., Bogorad, R.L., Sancak, Y., Kamer, K.J., Strittmatter, L., Li, A.A., Girgis, H.S., Kuchimanchi, S., De Groot, J., Speciner, L., et al. (2013). MICU2, a paralog of MICU1, resides within the mitochondrial uniporter complex to regulate calcium handling. PLoS ONE *8*, e55785. http://dx.doi.org/10.1371/journal.pone.0055785.

Poburko, D., Santo-Domingo, J., and Demaurex, N. (2011). Dynamic regulation of the mitochondrial proton gradient during cytosolic calcium elevations. J. Biol. Chem. *286*, 11672–11684.

Pralong, W.F., Spät, A., and Wollheim, C.B. (1994). Dynamic pacing of cell metabolism by intracellular Ca2+ transients. J. Biol. Chem. *269*, 27310–27314.

Rizzuto, R., Brini, M., Murgia, M., and Pozzan, T. (1993). Microdomains with high Ca2+ close to IP3-sensitive channels that are sensed by neighboring mitochondria. Science *262*, 744–747.

Rizzuto, R., Bastianutto, C., Brini, M., Murgia, M., and Pozzan, T. (1994). Mitochondrial Ca2+ homeostasis in intact cells. J. Cell Biol. *126*, 1183–1194.

Rizzuto, R., Pinton, P., Carrington, W., Fay, F.S., Fogarty, K.E., Lifshitz, L.M., Tuft, R.A., and Pozzan, T. (1998). Close contacts with the endoplasmic reticulum as determinants of mitochondrial Ca2+ responses. Science *280*, 1763–1766.

Robb-Gaspers, L.D., Burnett, P., Rutter, G.A., Denton, R.M., Rizzuto, R., and Thomas, A.P. (1998). Integrating cytosolic calcium signals into mitochondrial metabolic responses. EMBO J. *17*, 4987–5000.

Ryan, M.T., Voos, W., and Pfanner, N. (2001). Assaying protein import into mitochondria. Methods Cell Biol. *65*, 189–215.

Sato, T., and Mihara, K. (2010). Mammalian Oxa1 protein is useful for assessment of submitochondrial protein localization and mitochondrial membrane integrity. Anal. Biochem. *397*, 250–252.

Sparagna, G.C., Gunter, K.K., Sheu, S.S., and Gunter, T.E. (1995). Mitochondrial calcium uptake from physiological-type pulses of calcium. A description of the rapid uptake mode. J. Biol. Chem. *270*, 27510–27515.

Spät, A., Szanda, G., Csordás, G., and Hajnóczky, G. (2008). High- and low-calcium-dependent mechanisms of mitochondrial calcium signalling. Cell Calcium *44*, 51–63.

Szabadkai, G., Bianchi, K., Várnai, P., De Stefani, D., Wieckowski, M.R., Cavagna, D., Nagy, A.I., Balla, T., and Rizzuto, R. (2006). Chaperone-mediated coupling of endoplasmic reticulum and mitochondrial Ca2+ channels. J. Cell Biol. *175*, 901–911.

Szalai, G., Krishnamurthy, R., and Hajnóczky, G. (1999). Apoptosis driven by IP(3)-linked mitochondrial calcium signals. EMBO J. *18*, 6349–6361.

Tinel, H., Cancela, J.M., Mogami, H., Gerasimenko, J.V., Gerasimenko, O.V., Tepikin, A.V., and Petersen, O.H. (1999). Active mitochondria surrounding the pancreatic acinar granule region prevent spreading of inositol trisphosphate-evoked local cytosolic Ca(2+) signals. EMBO J. *18*, 4999–5008.

Trenker, M., Malli, R., Fertschai, I., Levak-Frank, S., and Graier, W.F. (2007). Uncoupling proteins 2 and 3 are fundamental for mitochondrial Ca2+ uniport. Nat. Cell Biol. *9*, 445–452.